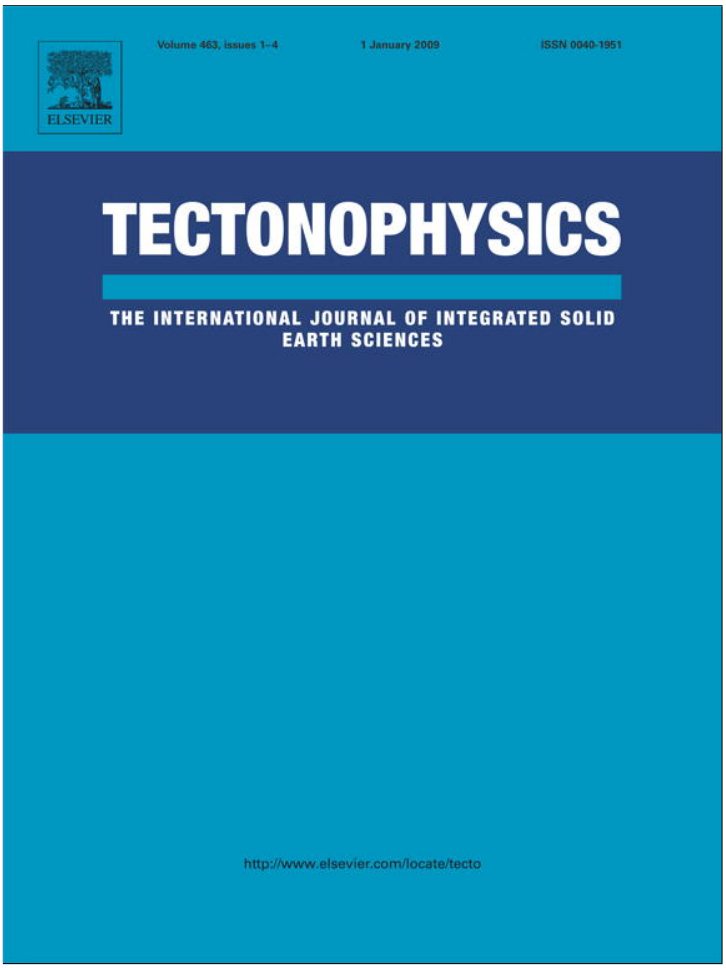

Tectonophysics 463 (2009) 130–144

Contents lists available at ScienceDirect

Tectonophysics

journal homepage: www.elsevier.com/locate/tecto

Recent seismicity and crustal stress field in the Lucanian Apennines and surrounding areas (Southern Italy): Seismotectonic implications

C. Maggi [a,b,*], A. Frepoli [a], G.B. Cimini [a], R. Console [a,b], M. Chiappini [a]

[a] Istituto Nazionale di Geofisica e Vulcanologia (INGV), via di Vigna Murata, 605, 00143, Rome, Italy
[b] Centro di Geomorfologia Integrata per l'Area del Mediterraneo (CGIAM), Potenza, Italy

ARTICLE INFO

Article history:
Received 18 August 2007
Received in revised form 29 August 2008
Accepted 17 September 2008
Available online 30 September 2008

Keywords:
Lucanian Apennines
Southern Italy
Seismicity
1D velocity model
Focal mechanisms
Stress field

ABSTRACT

We analyzed the instrumental seismicity of Southern Italy in the area including the Lucanian Apennines and Bradano foredeep, making use of the most recent seismological data base available so far. *P*- and *S*-wave arrival times, recorded by the Italian National Seismic Network (RSNC) operated by the Istituto Nazionale di Geofisica e Vulcanologia (INGV), were re-picked along with those of the SAPTEX temporary array deployed in the region in the period 2001–2004. For some events located in the upper Val d'Agri, we also used data from the Eni-Agip oil company seismic network. We examined the seismicity occurred during the period between 2001 and 2006, considering 514 events with magnitudes $M \geq 2.0$. We computed the V_P/V_S ratio obtaining a value of 1.83 and we carried out an analysis for the one-dimensional (1D) velocity model that approximates the seismic structure of the study area. Earthquakes were relocated and, for well- recorded events, we also computed 108 fault plane solutions. Finally, using 58 solutions, the most constrained, we computed regional stress field in the study area.

Earthquake distribution shows three main seismic regions: the westernmost (Lucanian Apennines) characterized by high background seismicity, mostly with shallow hypocenters, the easternmost below the Bradano foredeep and the Murge with deeper and more scattered seismicity, and finally the more isolated and sparse seismicity localized in the Sila Range and in the offshore area along the northeastern Calabrian coast. Focal mechanisms computed in this work are in large part normal and strike-slip solutions and their tensional axes (*T*-axes) have a generalized NE–SW orientation. The denser station coverage allowed us to improve hypocenters determination compared to those obtained by using only RSNC data, for a better characterization of the crustal and subcrustal seismicity in the study area.

1. Introduction

The Southern Apennines belong to the complex geodynamic setting characterizing the Central Mediterranean region, which is dominated by the NNW–SSE convergence between the European and African plates (Argus et al., 1989; De Mets et al., 1990). The tectonics of this area is accommodated by the collision between the Adriatic microplate and the Apenninic belt (Fig. 1). The eastward migration of the extension-compression system derived by the subduction process of the Adriatic microplate is related to the opening of the Tyrrhenian basin (Barberi et al., 2004). Seismological studies and recent geodetic observations reveal that the Apennines are undergoing a NE-trending extension, with seismic deformation rates higher in the southern portion (Di Luccio et al., 2005).

Highly energetic events in the last four centuries are historically well documented. The strongest events are localized in the Apenninic chain as, e.g., the 1694 earthquake that hit the Irpinia area and the 1857 Basilicata earthquake, located in the upper Val d'Agri and Vallo di Diano, both with effects of the XI degree on the Mercalli–Cancani–Sieberg (MCS) scale. The latest strong earthquake hit the Irpinia area in 1980 with effects of the X degree MCS and normal mechanism of rupture (Boschi et al., 1990) (Fig. 2). On the contrary, the foredeep and foreland areas to the South of the Ofanto river do not show considerable historical earthquakes with the exception of the 1560 event that hit the towns of Barletta and Bisceglie with effects of the VIII degree MCS.

From the instrumental seismic catalogue 1981–2002 (Castello et al., 2005) it appears that most of the background seismicity is located along the Apenninic chain (Fig. 2). Three main clusters of earthquakes are observable. The first, in the Potentino area, wherein which concentrated the earthquakes of the two seismic sequences occurring in the years 1990 (Azzara et al., 1993; Ekström, 1994) and 1991 (Ekström, 1994), both produced by E–W oriented strike-slip structures, and the second, in the Irpinia region. Finally, the last cluster in the Castelluccio area (1998 seismic sequence) with pure normal focal mechanism, close to the North-western border of the Pollino range

* Corresponding author. Istituto Nazionale di Geofisica e Vulcanologia (INGV), via di Vigna Murata, 605, 00143, Rome, Italy. Tel.: +39 06 51860649; fax: +39 06 51860397.
E-mail address: maggi@ingv.it (C. Maggi).

0040-1951/$ – see front matter © 2008 Elsevier B.V. All rights reserved.
doi:10.1016/j.tecto.2008.09.032

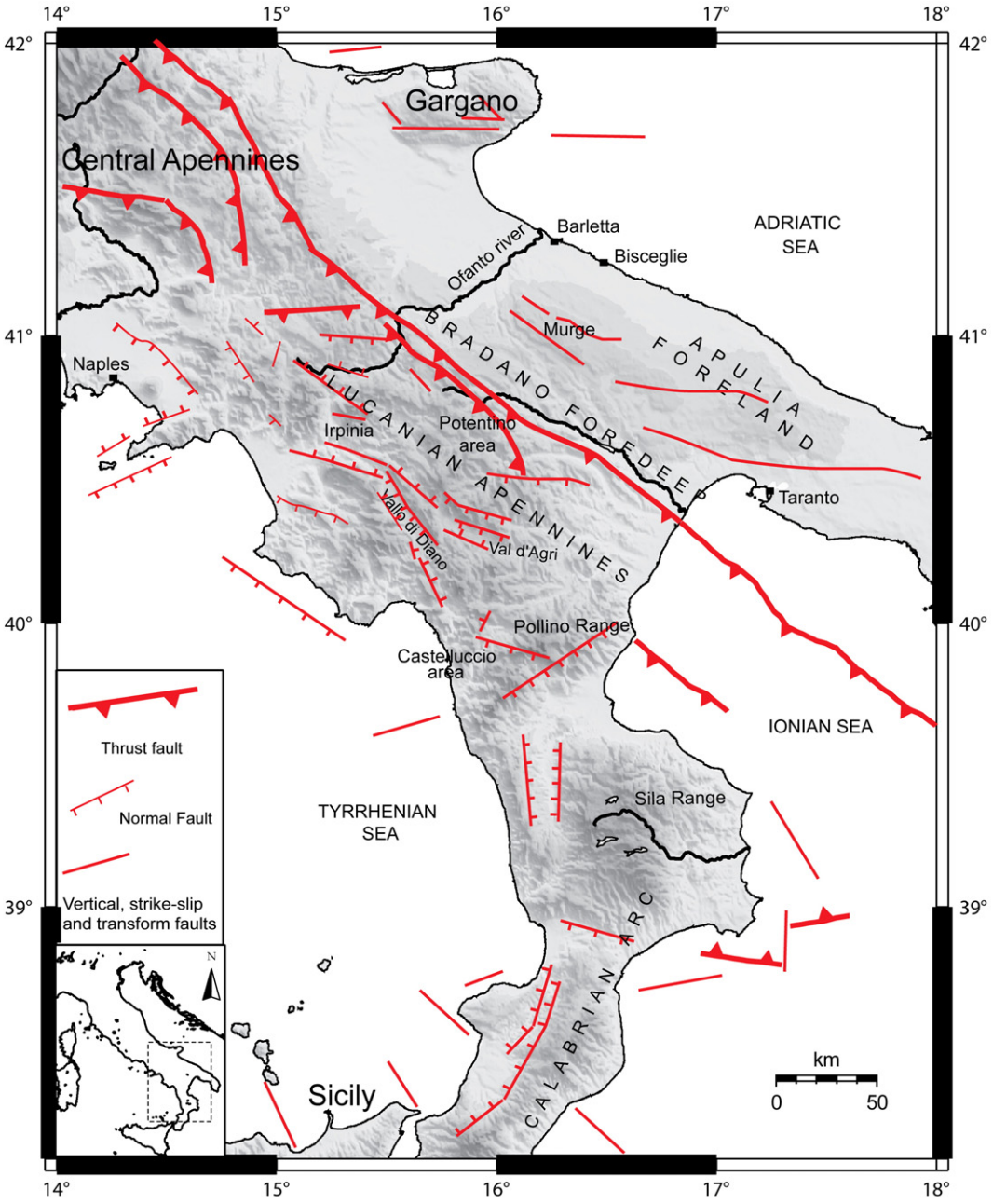

Fig. 1. Structural-kinematic map of Southern Italy (simplified from the "Structural map of Italy"; Bigi et al., 1990).

(Michetti et al., 2000; Pondrelli et al., 2002). The seismicity in the area between the Vallo di Diano and the upper Val d'Agri is sparse as in the external areas of the Bradano foredeep and the Apulia foreland.

The area of the Lucanian Apennines is one of the main seismically active regions of Southern Italy. The main goal of this paper is to provide new insights on the seismotectonic in this portion of the Apenninic chain through a careful analysis of background seismicity and active stress field information retrieved from fault plane solution inversion. Present-day stress field data are important for the seismotectonic zonation, a basic tool for seismic hazard evaluation, and are helpful to predict the behaviour of seismogenic faults. Taking advantage of the availability of a denser coverage of seismic stations in the area, we created a high quality database of local earthquake waveforms recorded during 2001–2006 by the RSNC, the SAPTEX temporary array (2001–2004) (Cimini et al., 2006), and the local ENI-AGIP network in the upper Val d'Agri (Fig. 3). This work is subdivided into four steps: (1) *Vp*/*Vs* ratio computation using a modified Wadati method, (2) application of the VELEST code (Kissling et al., 1995) to find the best one-dimensional (1D) velocity model for the study area, (3) relocation of the well-recorded events with the HYPOELLIPSE code (Lahr, 1989) to obtain a detailed seismicity distribution of earthquakes; and (4) focal mechanisms and regional stress field computation.

2. Data selection and *Vp*/*Vs* ratio computation

We re-picked arrival times of earthquakes recorded by the RSNC seismic network and picked those recorded by the temporary SAPTEX network in the period between June 2001 and December 2006. The ENI-AGIP network data were used only for some events located in the upper Val d'Agri and surrounding areas. During the observing period, the permanent network RSNC improved significantly in Southern Italy, increasing both the station coverage and the number of three-component extended band (Lennartz 5 s) or broad band (Trillum 40 s) sensors, which replaced the Kinemetrics S-13 short period sensors.

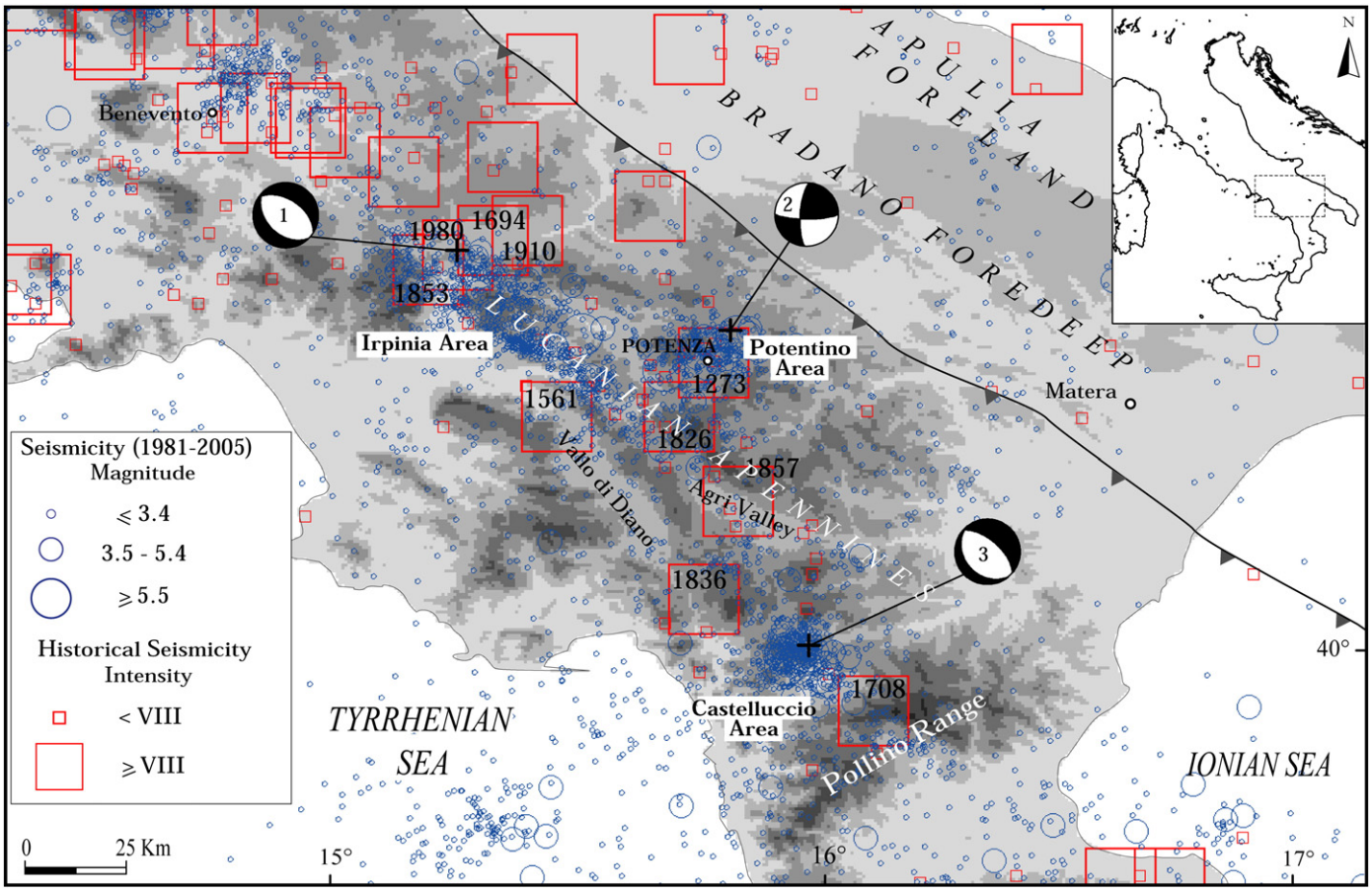

Fig. 2. Seismicity of Southern Italy from 1981 to 2005 (CPTI Working Group, 1999; Castello et al., 2005). Historical earthquakes are shown with the year of occurrence inside the unfilled red squares with size proportional to the estimated magnitude. Southern Apennines focal mechanisms of the three largest events occurred within the last three decades are also shown: 1) Irpinia area, 1980, Mw 6.9; 2) Potentino area, 1990, Mw 5.7; 3) Castelluccio area, 1998, Mw 5.6.

The ENI-AGIP stations are all equipped with three-component Lennartz Lite 1 s sensors. Both RSNC and ENI-AGIP networks record in trigger mode. The SAPTEX stations were equipped with three-component Lennartz 5 s sensors and the recording was set in continuous mode for tomographic analysis purpose (Frepoli et al., 2005; Cimini et al., 2006). The database we created is made up by 7570 *P*- and 4956 *S*-phases associated to 514 earthquakes with local magnitude $M_L \geq 2.0$. Only few events included in this database, and relocated with quite a high number of stations, have $M_L < 2.0$. We assigned a weight to each *P* or *S* arrival on the basis of picking accuracy (see Table 1).

To improve the hypocentral depth determination, an average V_P/V_S ratio is calculated using a modified Wadati method (Chatelain, 1978) shortly described below.

If we consider an event *k* that is recorded by two stations (*i*,*j*) at hypocentral distances x_i and x_j, the time difference between phases $P_i - P_j$ and $S_i - S_j$ can be expressed as:

$$DT_P = P_i - P_j = (x_i - x_j)/V_P \quad (1)$$

and

$$DT_S = S_i - S_j = (x_i - x_j)/V_S \quad (2)$$

where V_P and V_S are the *P*- and *S*-wave velocity values, respectively. Dividing (2) by (1) we obtain:

$$\frac{DT_S}{DT_P} = \frac{V_P}{V_S} \quad (3)$$

Fitting DT_S versus DT_P for all available pairs of stations gives the value of the slope V_P/V_S. We selected DT_S/DT_P according to the method used by Pontoise and Monfret (2004). From our data we obtain a V_P/V_S ratio of 1.83 with 95% prediction bounds, root mean square error (rms) of 0.40, and linear correlation coefficient (*R*) of 0.87 (Fig. 4). This value is quite similar to that obtained by other studies in the same region ($V_P/V_S = 1.82$, Frepoli et al., 2005). The presence of highly fractured zones related to the main faulting pattern in the study area (Gentile et al., 2000) could determine the relatively high value of the V_P/V_S ratio we found.

3. Minimum 1D velocity model

In order to better constrain the hypocentral locations we performed an analysis for the best *P*-wave one-dimensional (1D) velocity model of the study area, using the VELEST algorithm (Kissling et al., 1995). This velocity model together with station corrections can be used to relocate earthquakes with HYPOELLIPSE. Previous studies do not show a 1D model calculated in the restricted area of the Lucanian Apennines. Through VELEST we search a 1D velocity model that minimizes the least square solution to the coupled hypocentral–velocity model parameter solution. As this procedure does not invert for changes in layer thickness, we started from several initial models with varying thickness. In this way we introduced some layers with thickness of 3 or 4 km, up to 30 km depth, and of 5 km for greater depths. To account for the station elevations, we included an additional layer with thickness of 2 km over the sea level and $V_P = 5$ km/s.

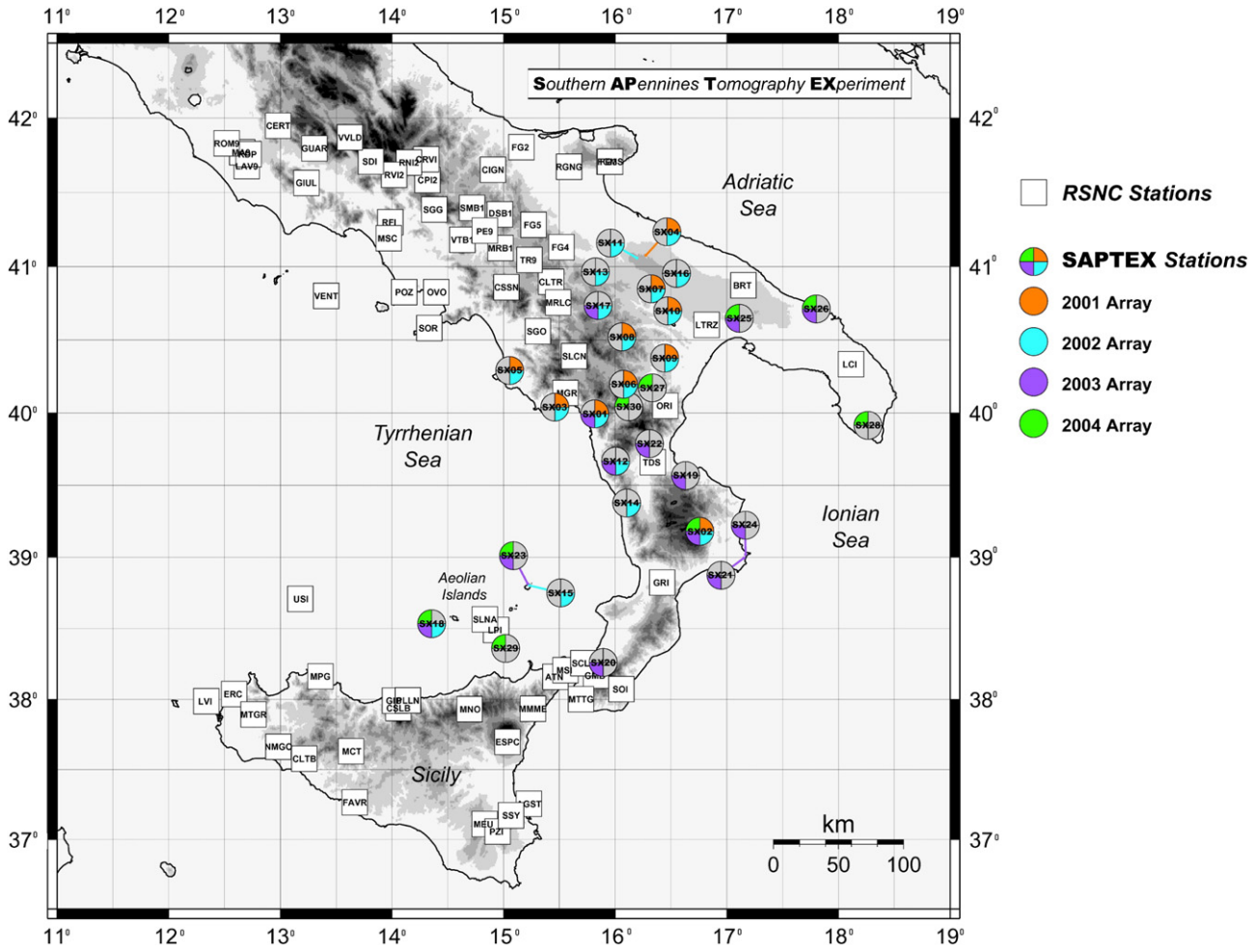

Fig. 3. Italian National Seismic Network (RSNC) and SAPTEX temporary seismic stations used in the study. White squares show the permanent stations of the RSNC and circles show the temporary stations deployed for the SAPTEX tomographic experiment during 2001 (orange), 2002 (blue), 2003 (magenta), and 2004 (green) (Cimini et al., 2006).

We used three different starting models: the first two were taken directly from the seismological literature as Chiarabba and Frepoli (1997) and Chiarabba et al. (2005), respectively. The latter is obtained using data of some Lucanian Apennine seismic studies (Merlini and Cippitelli, 2001; Cassinis et al., 2003; Barberi et al., 2004; Tiberti et al., 2005). We selected all the events with rms<1 s. We used mainly the direct *P*-wave arrivals, recorded by stations with a maximum epicentral distance around 300 km. All the selected earthquakes show an average azimuthal gap of 133°.

3.1. Starting models

The first starting model for Southern Italy was computed by Chiarabba and Frepoli (1997), and it is made of seven layers with a linear increase of velocity with depth. For this model we increased the number of layers (*Model1*). Adjacent layers not resolved by the data are merged into a single layer during VELEST iterations. In this way, using 308 selected events of our dataset, we computed the 1D velocity model *Vel_9* (Fig. 5a) with an average rms equal to 0.35 s. This model shows a Moho at 40 km depth. Fig. 5b shows large amounts of earthquakes in the depth interval 3–14 km, while at greater depth intervals the smaller amount of events does not allow for an improvement of the velocity model within the deeper layers.

The second starting model is a regional model computed by Chiarabba et al. (2005) for the entire Italian region. It consists of seven layers and includes a velocity inversion at 20 km of depth, within the lower crust beneath the belt. We re-stratified the initial model to better estimate the depth of the main discontinuities. To this model (*Model2*) we applied the VELEST code obtaining the final model *Vel_8* (Fig. 6a). For the inversion we used 315 selected events. The final model shows a Moho at 34 km depth and the average rms is equal to 0.35 s. In this model we have a larger amount of earthquake hypocenters within the 13–34 km depth interval (Fig. 6b).

The third starting model, called *Test*, is obtained from some Lucanian Apennines seismic studies (Tiberti et al., 2005; Barberi et al., 2004; Cassinis et al., 2003; Merlini and Cippitelli, 2001). It is made of six layers with a linear increase of velocity with depth. The correspondent increased layer model is called *Teststra*. With VELEST iterations we merged adjacent layers not resolved by the data and computed the final model *Test_8* (Fig. 7a) using the 307 selected events. The Moho depth is at 35 km and the final rms is 0.35 s. Fig. 7b shows a large amount of earthquake hypocenters within the 11–23 km depth range.

Table 1
Weights assigned to each *P*- and *S*- arrival time on the basis of picking accuracy

Weights	Picking accuracy (*s*)
1	0.04
2	0.10
3	0.20
4	0.40

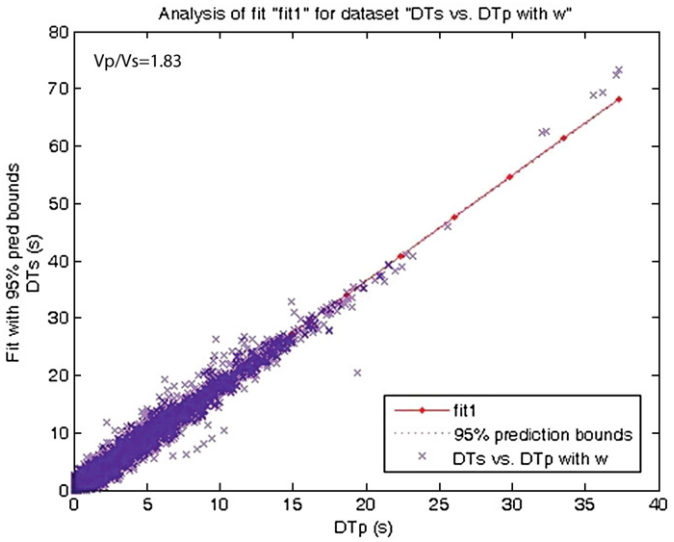

Fig. 4. V_P/V_S ratio for the Lucanian Apennines. Linear fit of DTs versus DT_P within 95% prediction bounds using Linear Least Squares Method. The root mean squared error (rms) is 0.40, and the linear correlation coefficient (R) is 0.87.

3.2. Model comparison

The study region is characterized by few deep events. For this reason we cannot well constrain the velocity model beneath the Moho. However, the main goal of this work is to obtain a model that approximates the real structure of this area within the crust. As shown in Fig. 8, the velocity of the three final models is similar especially where there is a larger amount of earthquakes. Moreover, models *Vel_8* and *Test_8* do not show evident velocity changes within the shallowest layer. The Moho depth (40 km) obtained in the model *Vel_9* is larger than the value estimated by previous studies. The wide angle reflection–refraction seismic exploration method (DSS) (Tiberti et al., 2005; Cassinis et al., 2003; Merlini and Cippitelli, 2001; Morelli, 1997) and the global model Crust2.0 (Bassin et al., 2000) find a Moho generally around 30–35 km depth. Moreover the crust beneath the Apenninic chain is characterized by a doubling of the Moho depth: the Tyrrhenian Moho depth increases from 15 to 25 km moving from the Tyrrhenian Sea to the ENE, while the Adriatic Moho deepens from 24 km under the Gargano promontory to 50 km under the Eastern margin of Tyrrhenian Sea (Ventura et al., 2007). The two models named *Vel_8* and *Test_8* show a Moho depth more consistent with that obtained from other studies (34 and 35 km of depth, respectively). For this reason, in the further steps of our work, we used these models for earthquakes relocation.

4. Earthquakes relocation

The seismicity studied in this paper occurred in the period between 2001 and 2006 and it is localized within a ~350×160 km NW–SE elongated region.

We relocated all the 514 events of our dataset with the HYPOELLIPSE code using the two models *Vel_8* and *Test_8*. We took into account earthquakes with azimuthal gap <180° and root mean square of the travel-time residuals rms <1.0 s. This value is obtained through the equation:

$$\mathrm{rms} = \left[\frac{\sum_i^n W_i R_i^2}{\sum_i^n W_i}\right]^{\frac{1}{2}} \quad i = 1,\ldots,n \tag{4}$$

where R_i is the residual of the ith phase and W_i is the computed weight of the ith phase. In this way we re-localized 337 events using model *Vel_8*, with an average rms=0.29 s and 359 earthquakes using model *Test_8*, with an average rms=0.30 s. Using the model *Vel_8* we obtain 61.1% of events with quality A and 20.2% with quality B. Whereas considering the second model (*Test_8*) we have 63.0% of earthquakes with quality A and 19.2% with quality B (see Table 2). Model *Test_8* is also consistent with the results of DSS studies (Cassinis et al., 2003) and with the recent European Crustal model (EuCRUST-07) (Tesauro et al., 2008) which indicate lower crust V_P velocity around 6.5 km/s and Moho depth of ca 35 km beneath the Apennines. Following these results we choose the model *Test_8* (Table 3) and its earthquakes relocation.

Using a denser station coverage, in comparison with that available in the past years, we obtained a significant improvement in the hypocentral locations. Analyzing the hypocentral distribution obtained using the velocity model *Test_8* (Fig. 9a and b), we observe that most of the earthquakes are localized beneath the Apenninic chain. The seismicity distribution enhances three main seismic zones. The westernmost of these is characterized by an earthquake distribution centred mainly along the axis of the Lucanian Apennine with maximum hypocentral depths up to 20 km (see Fig. 9b, sections AB, CD, EF and GH). Only few subcrustal events are present within this crustal domain. The second seismic zone is defined by a sparse and deeper seismicity (see Fig. 9a,b) localized within the eastern and outer margin of the chain and in the foredeep with depths up to 30 km. Finally, the last seismic zone (see Fig. 9b, section IL and MN; cross-section MN has 200 km of width) is localized within the Sila Range

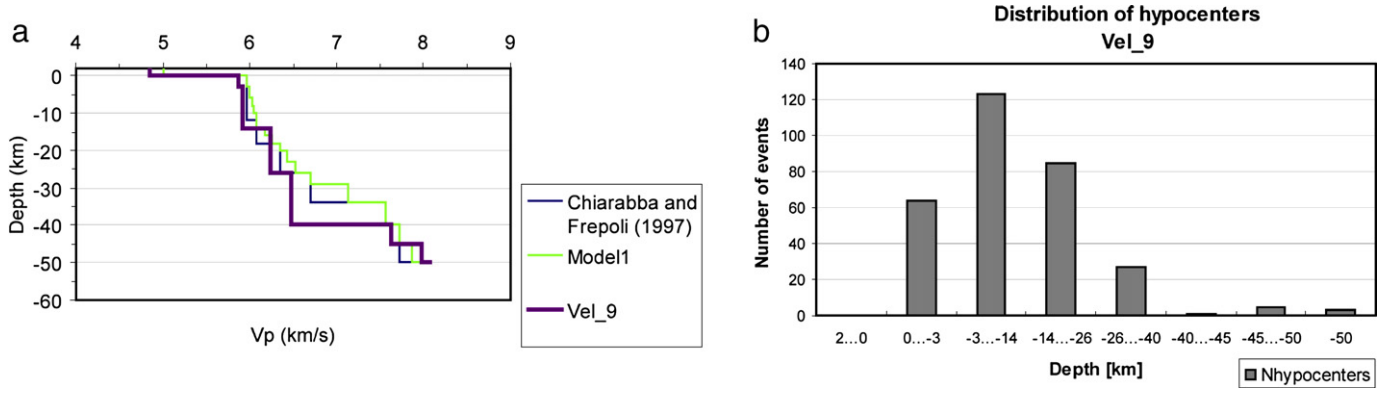

Fig. 5. a) Starting *P*-wave velocity model for the Italian region computed by Chiarabba and Frepoli (1997). We increased the number of layers: thickness of 3 or 4 km for each layer, up to 30 km depth, and of 5 km below 30 km depth. We named this model *Model1*. *Vel_9* is the final velocity model obtained with Velest. b) Hypocentral distribution versus depth for the model *Vel_9*.

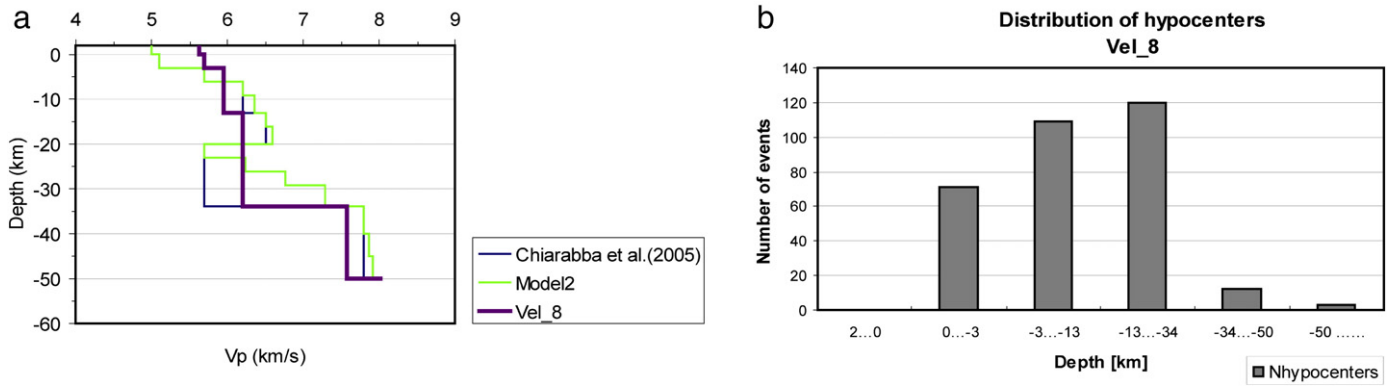

Fig. 6. a) Starting *P*-wave velocity model for the Southern Italy computed by Chiarabba et al. (2005). Number of layers are increased (see caption Fig. 5). We named this model *Model2*. *Vel_8* is the final velocity model obtained with Velest. b) Hypocentral distribution versus depth for the model *Vel_8*.

and the offshore northeastern Calabrian coast also characterized by a sparse seismicity and a maximum hypocentral depths around 30 km. Considering section MN in Fig. 9b which includes all the relocated earthquakes, the seismicity reaches 40 km beneath the Southern Apennines with an increase of hypocentral depth in the middle portion of the section, beneath the Lucanian region. This section shows two large clusters of hypocenters: one located in the Irpinia–Potentino area, and the other beneath the Moliterno–Pollino area. A seismic gap between the Pollino and the Sila Ranges is clearly observable. An isolated 88 km deep event belonging to the Southern Tyrrhenian subduction zone, is located beneath the Castelluccio area. This earthquake belongs to the sparse seismicity that characterizes the northern edge of the subduction zone. Fig. 10 shows the error ellipses with the 99% confidence limits of the relocated earthquakes. Events with D quality are excluded from this figure (see Table 2). Error ellipses are larger for events located where the angular distribution of the stations around the epicentre is sparse as in the Sila Range and in the Ionian Calabrian Coast. Our relocations are characterized by a large number of events with rms included in the 0.10–0.40 s interval. Most part of these events show maximum horizontal errors (Max_Err_H) smaller than 2.0 km and vertical errors (Err_Z) smaller than 3.0 km (Fig. 11). These results outline the high quality of our database.

5. Focal mechanisms and stress tensor inversion

5.1. Focal mechanism computation

We computed 108 first-motion focal mechanisms with at least eight clear observations using the FPFIT code (Reasenberg and Oppenheimer, 1985). From this dataset we selected 58 fault plane solutions with the two output quality factors Q_f and Q_p ranging from A to C for decreasing quality (Table 4). Q_f gives information about the solution misfit of the polarity data F_j, while Q_p reflects the solution uniqueness in terms of 90% confidence region on strike, dip and rake. The selected focal mechanisms for which A-A, A-B, B-A and B-B quality factors are obtained, are relatively well constrained (Table 5, Fig. 12a and b). Focal mechanisms with quality A-A are 31, and those with A-B and B-A are 27 (Table 5). All fault plane solutions with quality C for one of the two quality factors are rejected. The average number of polarities per event used in this study is 13. As shown from focal mechanisms of larger events, also from fault plane solutions of background seismicity we observe a widespread NE–SW extension in the Lucanian Apennine. Focal mechanisms calculated in this work are in large part normal and strike-slip solutions and their tensional axes (*T*-axes) have a generalized NE–SW orientation.

5.2. Stress tensor inversion

We applied the Gephart and Forsyth (1984) procedure, which was further implemented by Gephart (1990), to invert the focal mechanisms for the principal stress axes (σ_1, σ_2, σ_3) and the dimensionless parameter $R = \frac{(\sigma_2-\sigma_1)}{(\sigma_3-\sigma_1)}$ that describes the relative magnitudes of the principal stresses and hence constrains the shape of the deviatoric part of the stress tensor. The inverse method using focal mechanism data cannot determine the absolute magnitude of the deviatoric and isotropic stresses. It only can identify the best stress tensor model that most closely matches all the fault plane solutions of the source region. The method requires the basic assumptions that the stress is uniform

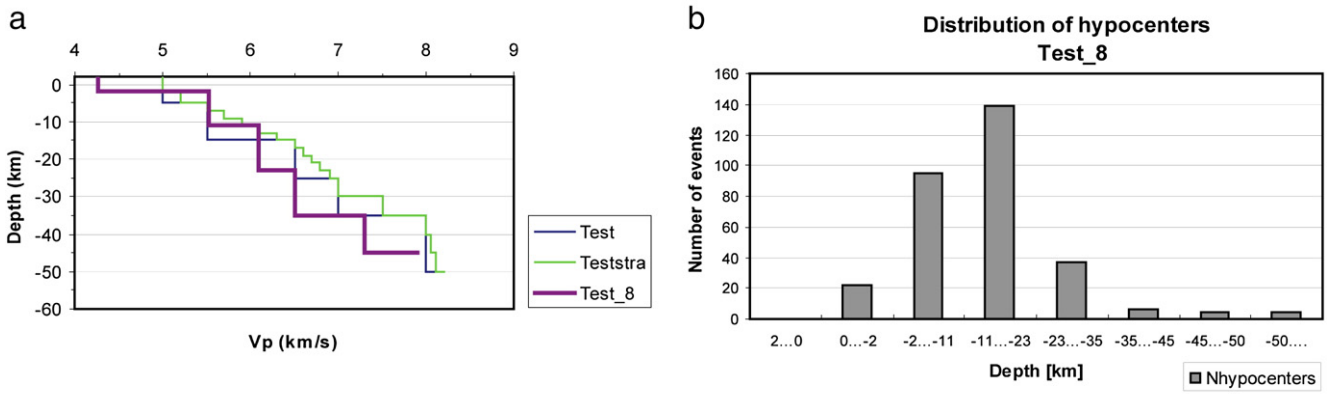

Fig. 7. a) Starting *P*-wave velocity model *Test* for the Lucanian Apennines. Number of layers are increased (see caption Fig. 5). We named this model *Teststra*. *Test_8* is the final velocity model obtained with Velest. b) Hypocentral distribution versus depth for the model *Test_8*.

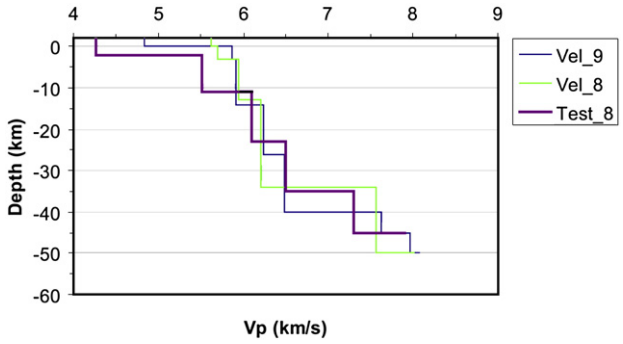

Fig. 8. *P*-wave velocity final models obtained by VELEST. *Vel_8* is the model derived from *Model2*, *Vel_9* from *Model1* and *Test_8* from *Teststra*.

in space and time in the investigated volume. The brittle shallow crust would include small pre-existing faults of any orientation that may have low frictional coefficients. Earthquakes are shear dislocations on these pre-existing faults and slip occurs in the direction of the resolved shear stress on the fault plane. Discrepancy between stress tensor orientation and an observation is defined by a misfit measure which is given by the angular difference between the observed slip direction on a fault plane and the shear stress on that fault plane derived from a given stress tensor. Misfit is computed through an angular rotation about an axis for both nodal planes of each focal mechanism on a grid search of stress tensors. The stress tensor orientation that provides the average minimum misfit is assumed to be the best stress tensor for a given population of focal mechanisms.

We excluded from the inversion procedure 9 focal mechanisms, out of the 58 best selected fault plane solutions, which do not belong to the shallower crustal seismicity (depth smaller than 30 km) located within the Apenninic chain. This allows us to define the boundary of smaller crustal volumes approaching better the assumption of the uniform spatial stress field. We performed first an inversion with 49 focal mechanisms, all located inside the Apenninic chain from the northern Pollino Range to the northern Irpinia area. The minimum average misfit is 7.7°, corresponding to a stress tensor with a horizontal σ_3 (plunge 4°) NE–SW directed, an NW–SE oriented σ_2 (plunge 43°) and a σ_1 (plunge 47°) (Fig. 13a). The 95% confidence intervals of the principal stress axes do not overlap, suggesting that the three axes are well constrained by the data. The stress ratio *R* near the solution is 0.7 denoting that σ_2 is slightly close in its absolute value to σ_3. Notwithstanding the good results in agreement with previous studies showing the general extension in a NE–SW direction of this part of the Apenninic chain, large misfits suggest an inhomogeneous stress distribution within the considered crustal volume (Wyss et al., 1992).

For this reason we performed two further inversions dividing the dataset into two sub-volumes (see Fig. 12a and b): one to the North, including the Irpinia and Potentino areas with 28 focal mechanisms, and the other to the South, including the Moliterno–Val d'Agri and the North-western Pollino Range with 21 fault plane solutions. In the Irpinia–Potentino the shape factor parameter *R* is between 0.4 and 0.5, while the misfit is 7.0°, suggesting a more homogenous stress field in this area. The minimum stress axis (σ_3) is sub-horizontal (plunge 14°) and NE–SW oriented and σ_1 is quite close to the vertical (75° of plunge) (Fig. 13b).

The inversion results for the Moliterno–Val d'Agri area and the North-western Pollino range show a stress tensor with an orientation very similar to that obtained by using the whole dataset. The σ_3 is NE–SW directed with 3° of plunge, while σ_1 is sub-vertical (58° of plunge) and NW–SE oriented (Fig. 13c). Also here *R* ratio is around 0.5, suggesting that the three principal stress axes are well separated in their absolute values. Moreover, the average misfit (6.0°) shows that the stress heterogeneities, inside the Southern sector, are smaller than in the previous areas.

Table 2
Quality based on the value of the horizontal error SEH (68% confidence limit), and vertical error SEZ (68% confidence limit)

Quality	Larger of SEH and SEZ	Model *Test_8*		Model *Vel_8*	
		Number of events	% number of events	Number of events	% number of events
A	≤1.34	226	63%	206	61.1%
B	≤2.67	69	19.2%	68	20.2%
C	≤5.35	31	8.6%	40	11.9%
D	>5.35	33	9.2%	23	6.8%

Table 3
Velocity values of the best model for Lucanian Apennines computed with VELEST code

Top of layer (km)	Velocity of model *Test_8* (km/s)
0	4.27
−2	5.52
−11	6.1
−23	6.5
−35	7.31
−45	7.9

6. Discussion and conclusions

The large number of stations available in the last years through the significant improvement of the RSNC spatial coverage and the deployment of the SAPTEX temporary array, allow us to obtain more constrained locations of low magnitude events in the Lucanian region compared to previous studies. We computed the V_P/V_S ratio, the 1D velocity model and station corrections valid for this region to improve the location of the background seismicity. The high value of the V_P/V_S ratio (1.83) might be associated to the presence of highly fractured zones.

The regional gravity anomaly maps and DSS study outlined the existence of a doubling of the Moho beneath the Lucanian Apennines (Morelli, 2000; Tiberti et al., 2005). This area is characterized by a relative gravity low surrounded by areas with gravity high. This is likely related to the overlap of the Tyrrhenian and Adriatic Moho (Speranza and Chiappini, 2002; Tiberti et al., 2005) beneath the Apenninic chain that would be associated to the subduction process. Through our analysis we obtained a model in which the average Moho is set at 35 km depth, in agreement with the average depth defined for the Southern Apennines in previous works (Locardi and Nicolich, 1988; Cassinis et al., 2003). The average *P*-wave velocity (V_P=7.31 km/s) observed at the Moho discontinuity in our analysis is slightly lower than the average value (V_P=7.56 km/s) computed by Chiarabba and Frepoli (1997) for the Southern Italian region.

Despite the short time interval of observation, the seismicity examined in this work is representative of the seismic behavior of the Lucania and surrounding regions as known from a longer period of data collection (Castello et al., 2005). In fact, the spatial distribution of the analyzed events closely follows the pattern delineated by the seismicity of the last two decades (Fig. 2).

In particular we find that the seismicity is clustered in the Potentino and Irpinia area to the North, and in the Moliterno and North-western Pollino Range to the South. This result enhances the presence of a seismic gap located in the Vallo di Diano and upper Val d'Agri area characterized by very low and sparse background seismicity. Following the macroseismic data and the most recent geological and geomorphological studies (Maschio et al., 2005) the seismogenic structure related to the 1857 Basilicata earthquake (XI MCS) is hypothesized in this area. The eastern margin of the chain and

the Bradano foredeep are characterized by a more sparse seismicity which shows larger hypocentral depths (generally between 20 and 30 km) than those observed in the inner portion of the chain (generally between 5 and 20 km).

This eastward deepening of the hypocentral depths, from the inner to the outer margin of the belt, indicates a deeper boundary between the brittle and ductile crust beneath the external margin of the Lucanian Apennine and the foredeep, compared to that beneath the chain itself. This increasing seismogenic layer depth is associated with the westward flexural bending of the Adriatic continental lithosphere beneath the Apenninic chain (Chiarabba et al., 2005). Tomographic and geothermal gradient studies point out a brittle–ductile transition at 28–30 km beneath the foredeep and foreland compared with the 15–18 km of depth of the same limit beneath the chain (Harabaglia et al., 1997; Chiarabba and Amato, 1996). These data, together with positive Bouger anomalies, are consistent with the presence of an uprising asthenospheric material in the upper mantle below the Tyrrhenian margin of the chain and the adjacent Tyrrhenian Sea (Scrocca et al., 2005). Moreover, the doubling of the Moho beneath the Lucanian Apennines is interpreted as a "soft" asthenospheric wedge intruding between the down going Adriatic plate and the overriding plate (Ventura et al., 2007). The uplift and crustal thinning of the Apennines with the consequent active rifting processes along the chain axis are triggering the seismicity within the Apenninic chain. These considerations confirm the modern interpretation of the complex geodynamic setting characterizing the Central Mediterranean region, which is dominated by the NNW–SSE convergence between the Eurasia and Nubia (i.e., the African plate west of the East African Rift) plate (D'Agostino and Selvaggi, 2004). The recent interruption of the Southern Apenninic thrusting is probably due to collision of the subducting Adriatic microplate with the Apulian block

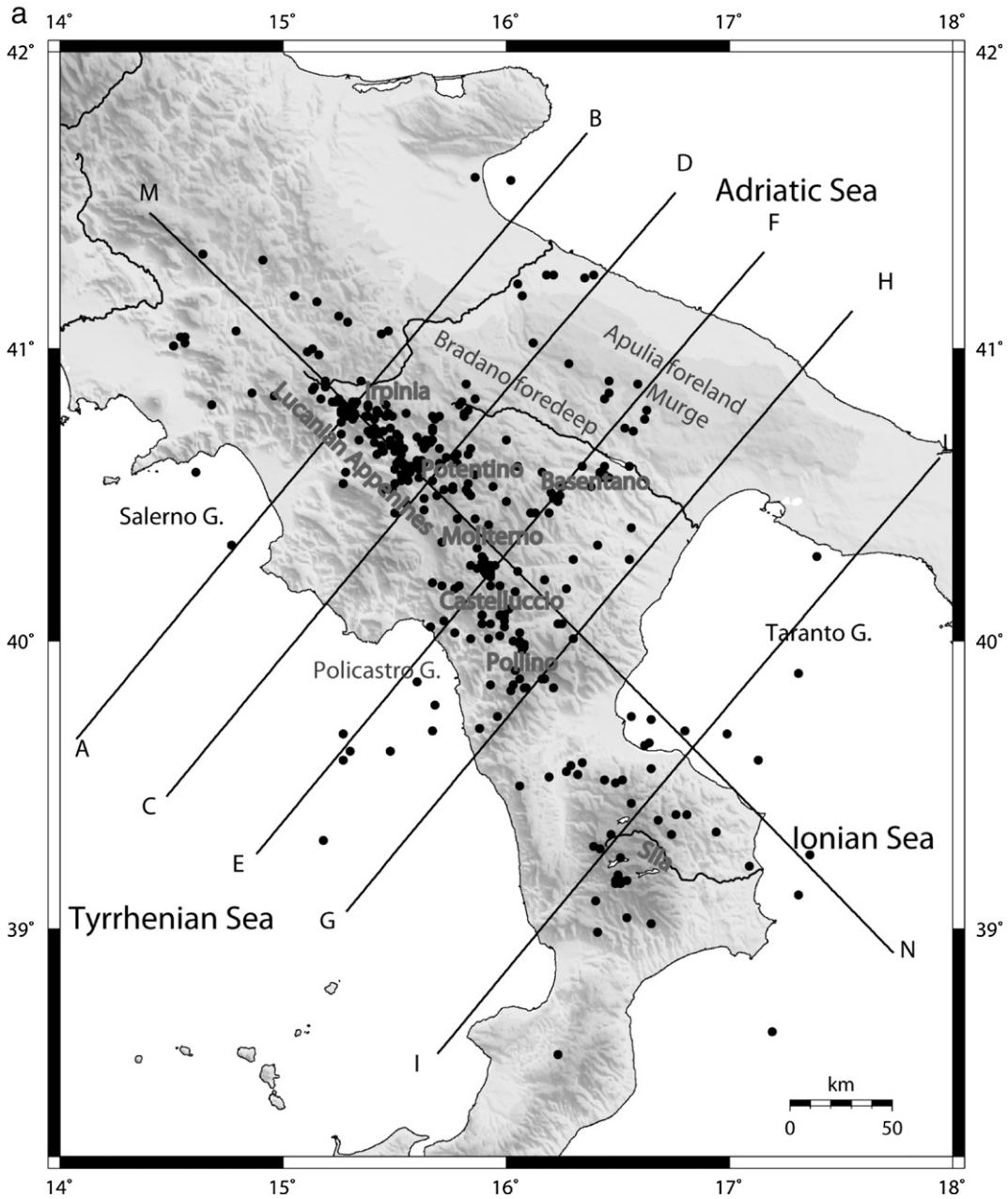

Fig. 9. a) Epicentral distribution of the 359 earthquakes located using the model *Test_8*. The width of cross-sections AB, CD, EF, GH, and IL is 25 km. The width of cross-section MN is 200 km. b) Cross-sections with depth ≤50 km.

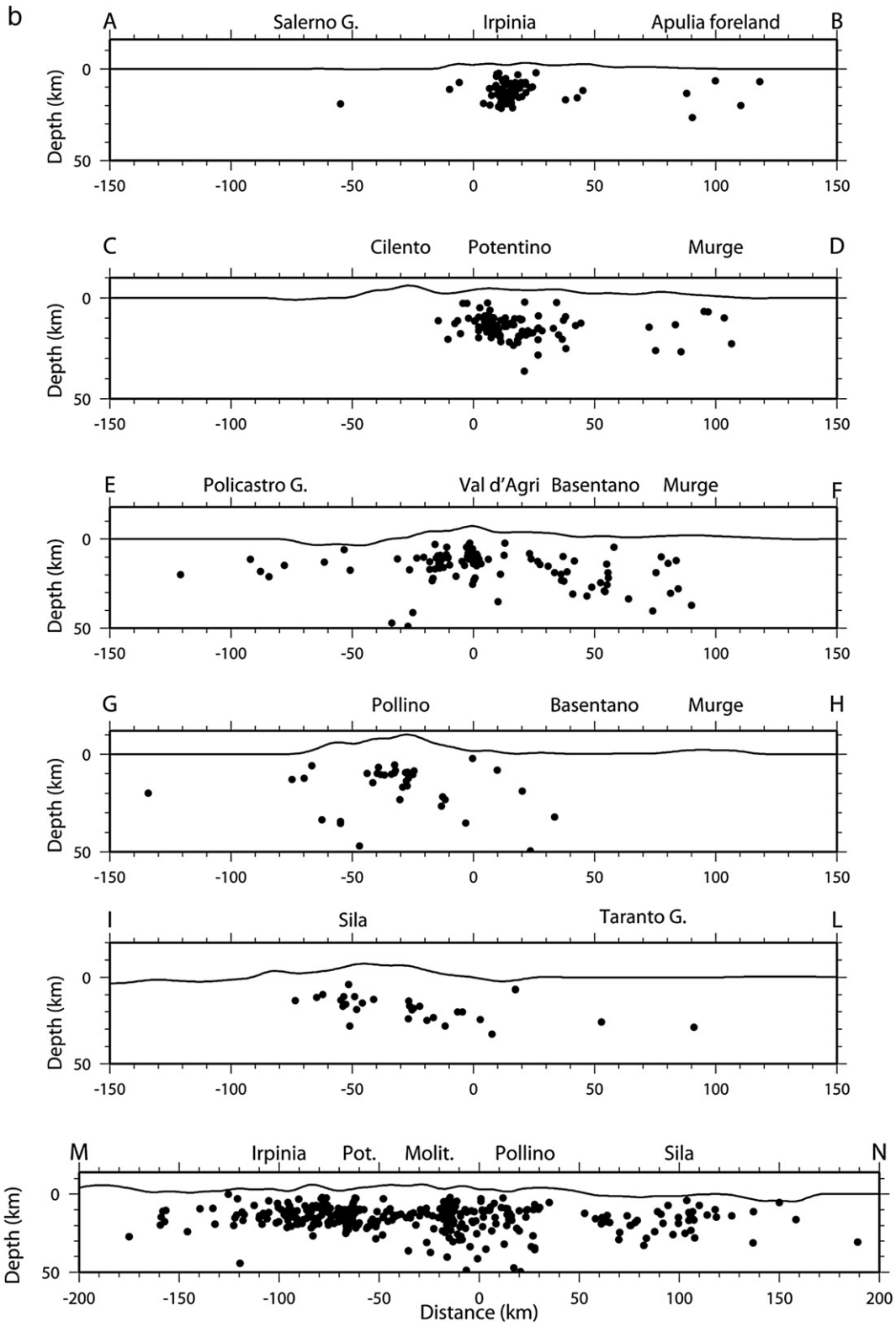

Fig. 9 (*continued*).

(Hollenstein et al., 2003) and it is related to the opening of the Tyrrhenian basin. This mechanism has produced a change of the previous compressional regime into the present extensional regime along all the Apenninic arc during the Middle Pleistocene (Hyppolite et al., 1994).

In our analysis 49 events beneath the Apenninic chain and the Bradano foredeep show depths larger than 23 km. Among them, the deepest event is located at ~49 km depth beneath the area of Policoro–Montalbano Jonico, with quality A. This sparse deep seismicity could be explained as a result of the retreat of the

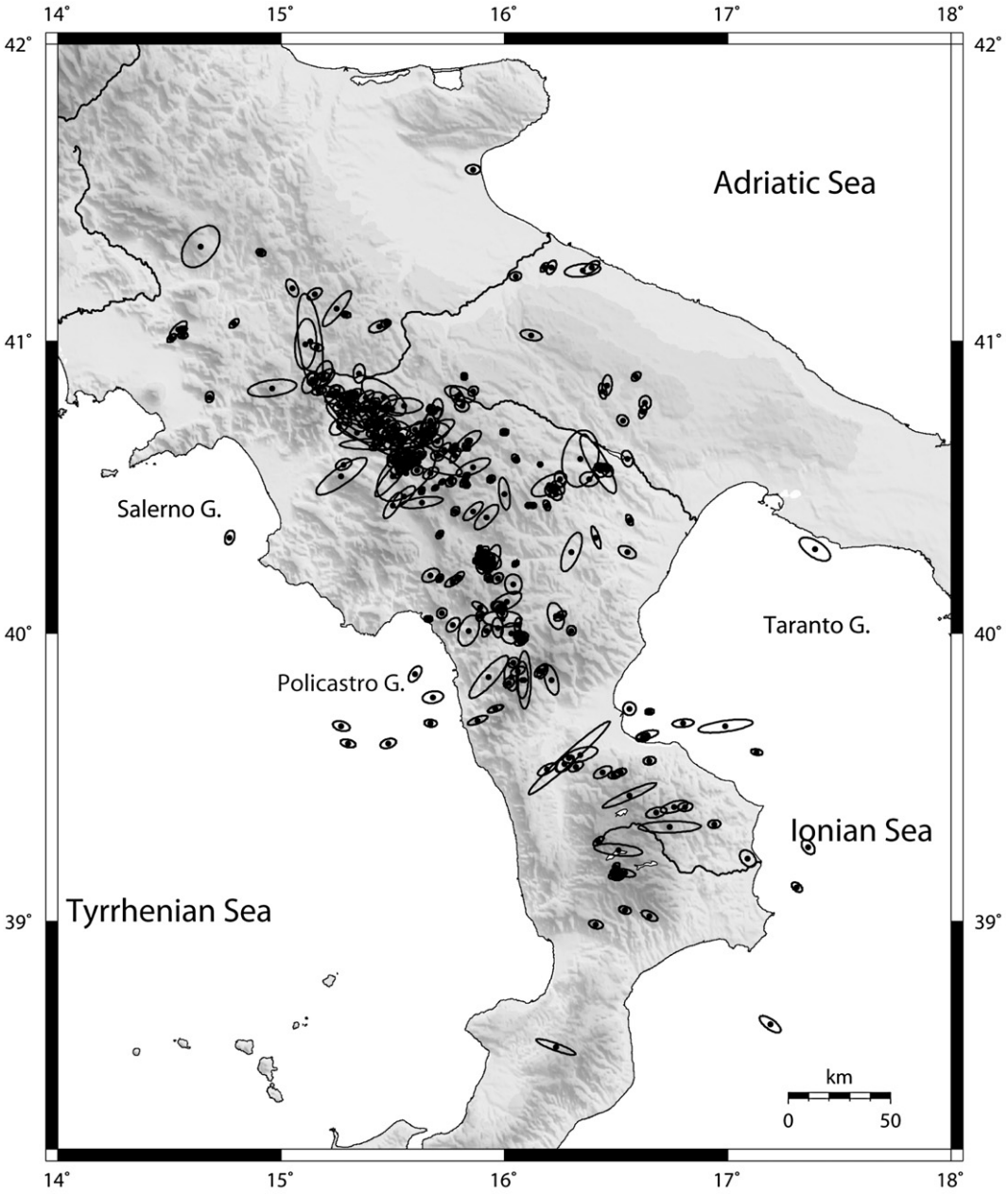

Fig. 10. Earthquake location and error ellipse (99% confidence limit): events with quality A, B and C.

subducting Adriatic lithosphere (Malinverno and Ryan, 1986; Amato et al., 1993) as shown in the northern Apenninic chain.

We analyzed also the seismicity south of the Pollino Range (Fig. 9a). Here the background seismicity is concentrated in the Sila Range and in the offshore sector of the Ionian Sea, close to the northeastern Calabrian coast (Taranto Gulf). The Castrovillari (Southern Pollino Range) and Piana di Sibari areas appear to be characterized by lack of seismicity.

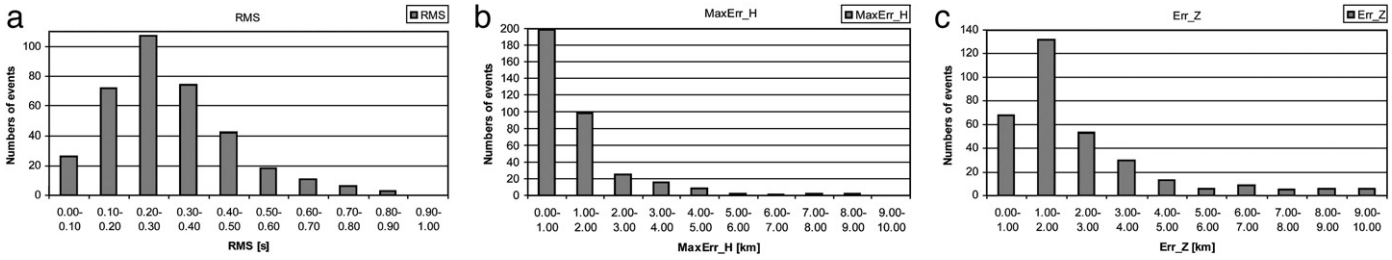

Fig. 11. Distribution of: a) rms; b) maximum horizontal error (Max_Err_H) and c) vertical error (Err_Z) for relocated events. In b) and c) we considered only events with horizontal and vertical errors less than 10 km.

Table 4
Value of quality factor Q_f and Q_p for fault plane solution

Quality	Q_f	Q_p
A	$F_j \leq 0.025$	Δs, Δd, Δr ≤ 20°
B	$0.025 < F_j \leq 0.1$	20° to 40°
C	$F_j > 0.1$	>40°

$F_j = 0$ indicates a perfect fit to the data, while $F_j = 1$ is a perfect misfit. Δs, Δd and Δr are ranges of perturbation of strike, dip and rake, respectively.

The distribution of focal mechanisms of background seismicity is helpful in delineating the main seismotectonic provinces of the study region. Our results point to an active extensional regime in this part of the Apenninic chain. Fault plane solutions computed in this work show tensional axes (*T*-axes) generally NE–SW oriented. This widespread NE–SW extension is consistent with previous studies concerning focal mechanisms of low to moderate magnitude events (Frepoli and Amato, 2000; Frepoli et al., 2005), fault

Table 5
Southern Italy fault plane solutions selected

No.	Date	O.T.	Latitude	Longitude	Depth	M_L	rms	ERH	ERZ	strike	Dip	Rake	Q_f	Q_p	N. P.	Category	Area
1	010914	08:02	40° 37.64	15° 43.67	20.81	2.4	0.38	0.8	0.7	120	45	−130	A	A	11	NF	Potentino
2	011104	10:22	40° 26.10	16° 06.65	12.32	2.1	0.62	0.4	1.0	130	20	−130	A	A	11	NF	Dolomiti Lucane
3	011104	10:28	40° 26.45	16° 07.53	14.19	2.3	0.60	0.3	1.1	110	30	−100	B	A	16	NF	Dolomiti Lucane
4	011113	13:21	40° 31.93	15° 56.46	36.15	1.9	0.79	0.5	0.8	130	65	150	A	A	13	SS	Potentino
5	011121	06:21	40° 32.14	15° 49.99	13.11	2.3	0.26	0.4	1.2	125	40	−120	A	B	12	NF	Potentino
6	011209	12:15	40° 47.72	15° 17.23	16.63	3.3	0.31	0.5	1.0	130	20	−80	B	A	15	NF	Irpinia
7	020102	02:17	40° 46.72	15° 25.04	15.40	2.8	0.23	0.6	1.5	140	75	−80	A	A	9	NF	Irpinia
8	020208	04:38	40° 15.45	15° 55.48	11.24	2.2	0.19	0.5	3.3	150	55	−60	A	A	10	NF	Moliterno
9	020226	17:12	40° 14.52	15° 55.59	5.45	2.1	0.29	0.3	0.8	15	40	−20	A	A	9	U	Moliterno
10	020402	04:22	40° 16.15	15° 53.45	13.70	2.7	0.66	0.4	1.3	165	85	−100	A	A	14	U	Moliterno
11	020413	08:44	40° 30.32	15° 49.80	13.12	2.4	0.30	0.4	1.3	120	75	−170	A	A	13	SS	Potentino
12	020413	10:48	40° 11.39	15° 55.51	12.36	2.1	0.21	0.5	1.1	285	60	−160	A	B	8	SS	Moliterno
13	020413	17:04	40° 33.91	16° 25.11	29.33	3.0	0.40	0.4	0.8	350	60	−120	A	A	32	NF	Basentano
14	020413	20:28	40° 33.60	16° 26.07	28.87	2.1	0.25	0.9	3.4	130	65	−110	A	B	8	NF	Basentano
15	020418	21:00	40° 35.30	15° 34.13	10.28	3.0	0.28	0.4	0.5	200	75	−10	A	B	17	SS	Savoia di Lucania
16	020418	21:36	40° 34.96	15° 34.39	9.60	2.2	0.24	0.6	0.5	200	80	−10	A	B	13	SS	Savoia di Lucania
17	020418	22:58	40° 35.00	15° 34.23	9.47	2.7	0.29	0.4	0.5	100	80	150	A	B	12	SS	Savoia di Lucania
18	020419	18:06	40° 35.72	15° 34.05	6.00	2.5	0.24	0.6	2.9	170	50	−50	A	A	10	NF	Savoia di Lucania
19	020504	09:41	40° 39.65	15° 32.20	15.77	2.3	0.39	0.4	1.1	160	45	−50	B	A	11	NF	Irpinia
20	020505	06:40	40° 37.31	15° 37.32	21.58	1.9	0.24	0.6	0.9	155	50	−150	A	A	8	NS	Irpinia
21	020508	19:29	40° 05.32	15° 59.62	14.50	2.9	0.29	0.4	1.1	280	85	−130	B	A	21	U	Northern Pollino
22	020512	20:20	40° 38.15	15° 46.51	18.47	2.1	0.32	0.4	1.0	100	65	170	A	B	11	SS	Potentino
23	020526	10:19	40° 32.96	15° 32.02	11.38	2.6	0.30	0.5	1.4	140	45	−70	A	A	8	NF	Vallo di Diano
24	020531	16:31	40° 14.93	15° 54.59	10.38	2.5	0.20	0.4	0.5	140	70	−40	B	A	13	NS	Moliterno
25	020611	20:02	40° 31.13	15° 43.45	13.97	2.1	0.45	0.3	0.6	140	50	−130	B	A	19	NF	Potentino
26	020618	23:31	40° 31.73	15° 45.47	10.97	2.3	0.37	0.3	0.5	255	75	0	A	A	19	SS	Potentino
27	020621	19:34	40° 05.56	15° 58.90	10.55	2.4	0.42	0.4	0.6	10	35	−20	B	A	13	U	Northern Pollino
28	020623	21:41	41° 15.02	16° 23.52	22.65	2.8	0.29	0.9	1.0	90	60	160	A	A	10	SS	Murge
29	020712	11:12	39° 59.24	16° 04.04	16.16	3.2	0.31	0.6	2.7	65	55	−80	A	A	13	NF	Northern Pollino
30	020713	05:57	39° 59.24	16° 03.42	9.22	2.1	0.47	0.4	0.7	145	30	−60	A	A	11	NF	Northern Pollino
31	020713	11:49	39° 58.52	16° 04.54	13.65	2.7	0.35	0.6	3.8	105	45	−100	A	A	8	NF	Northern Pollino
32	020718	08:28	39° 59.94	16° 03.61	9.01	2.5	0.46	0.4	0.7	100	45	−110	A	A	9	NF	Northern Pollino
33	020815	12:58	39° 44.47	15° 57.67	35.26	2.1	0.66	0.7	0.8	35	75	−170	A	B	12	SS	Orsomarso
34	020815	14:37	39° 44.16	15° 57.61	34.21	3.0	0.60	0.6	0.7	45	80	−150	B	A	20	SS	Orsomarso
35	020903	01:45	40° 30.11	15° 41.12	14.82	1.9	0.35	0.4	0.5	85	65	−130	B	A	16	NF	Potentino
36	021004	22:58	40° 15.13	15° 55.71	10.83	2.9	0.32	0.5	0.4	320	85	10	A	A	18	SS	Moliterno
37	021006	02:43	40° 14.41	15° 55.23	10.48	1.9	0.21	0.5	0.6	135	50	−60	A	A	12	NF	Moliterno
38	021109	01:53	40° 49.70	15° 51.78	13.52	2.0	0.25	0.6	1.9	145	60	−60	A	A	8	NF	Potentino
39	021119	16:53	40° 14.25	15° 55.05	8.98	1.8	0.19	0.5	1.1	50	80	0	A	A	10	SS	Moliterno
40	021129	10:54	40° 14.12	15° 55.04	10.50	1.9	0.22	0.5	0.9	40	70	0	A	A	9	SS	Moliterno
41	021130	01:19	40° 14.03	15° 54.69	10.57	2.4	0.23	0.4	0.6	120	40	−80	A	A	14	NF	Moliterno
42	021130	17:33	40° 13.84	15° 54.97	11.31	2.2	0.18	0.5	1.1	170	80	−40	B	A	13	SS	Moliterno
43	021201	00:30	40° 13.34	15° 55.54	7.58	2.1	0.28	0.3	0.8	5	50	−30	B	A	11	NS	Moliterno
44	021209	10:38	39° 10.24	16° 29.42	16.55	3.3	0.43	0.5	1.9	80	55	−60	B	A	14	NF	La Sila
45	030311	00:22	40° 53.06	16° 35.14	37.17	2.9	0.40	0.6	1.2	180	70	−40	B	A	16	NS	Murge
46	040224	05:21	40° 42.91	15° 24.39	16.51	3.8	0.26	0.7	1.5	135	25	−90	A	A	13	NF	Irpinia
47	040903	00:04	40° 41.25	15° 38.43	21.91	4.1	0.74	0.6	0.6	80	55	160	B	A	24	SS	Potentino
48	040903	01:22	40° 41.27	15° 39.87	10.75	2.8	0.24	0.7	0.7	20	55	−10	A	A	9	SS	Potentino
49	060107	04:27	40° 38.51	15° 49.77	17.21	2.3	0.23	0.5	2.2	25	50	−90	A	A	10	NF	Potentino
50	060314	03:15	40° 49.07	15° 19.58	10.46	2.7	0.29	0.4	0.6	155	50	−60	A	A	9	NF	Irpinia
51	060717	16:56	40° 46.46	15° 29.41	8.35	2.5	0.36	0.4	0.7	125	40	−90	A	B	9	NF	Irpinia
52	060907	15:31	40° 35.00	16° 09.53	30.70	3.9	0.41	0.3	0.6	65	25	−120	B	A	23	NF	Basentano
53	060915	17:55	40° 45.96	15° 23.03	16.17	2.4	0.17	0.6	1.6	70	85	−170	A	A	10	SS	Irpinia
54	060926	16:29	40° 43.32	15° 27.30	7.84	3.0	0.28	0.3	0.6	80	75	−110	B	A	15	NF	Irpinia
55	061022	00:38	40° 03.57	15° 53.35	16.98	2.4	0.25	0.6	1.1	25	45	−60	A	B	9	NF	Northern Pollino
56	061115	15:08	40° 20.24	15° 42.69	12.59	2.7	0.24	0.5	1.0	25	60	−90	A	A	10	NF	Vallo di Diano
57	061201	15:38	40° 46.48	15° 27.62	15.00	2.7	0.21	0.4	1.3	130	40	−120	A	A	12	NF	Irpinia
58	061205	06:20	41° 05.26	15° 17.29	16.73	2.5	0.41	0.5	1.1	175	70	−70	B	A	10	NF	Northern Irpinia

Date in format year-month-day; O.T = origin time (hour and minute); Latitude north and Longitude east; Depth in km; M_L = local magnitude of events belonging to the 2001–2002 period from the Italian Seismic Catalogue (CSI) and of 2003–2006 period from INGV Seismic Bulletin; rms = root mean square of residuals of relocation; ERH and ERZ = horizontal and vertical location errors; strike, dip and rake of the first nodal plane; Q_f and Q_p = focal mechanism quality factors based on misfit and confidence regions; N.P. = polarities number; category = fault plane solution type (SS = strike-slip, NS = normal fault with small strike-slip component, NF = normal fault, U = undefined solution category); Area = geographical locality of event epicenter.

plane solutions of larger earthquakes (Pondrelli et al., 2002) and breakout analyses (Cucci et al., 2004; Montone et al., 2004). It is well-known that the breakout method samples a depth interval between 3 and 6 km, suggesting a continuity in the stress regime at different depths.

A detailed knowledge of the active stress field is necessary in order to constrain the active tectonic processes and the recent geodynamic evolution of the Southern Italian region. The inversion performed with the largest fault plane solution dataset (49 events), which includes all the Lucanian Apennines from the Irpinia–Potentino area, to the North, to the North-western Pollino Range, to the South, gives a stress field with an oblique σ_1 and a sub-horizontal NE-directed σ_3. The relatively high average misfit value (7.7°), however, indicates an inhomogeneous stress distribution within the region under investigation. These results could be interpreted by taking into account that the stress field is influenced by second-order structural elements. For this reason we performed new inversions in order to better analyze the stress heterogeneity within the selected area. Taking into account the scarcity of background seismicity in the Vallo di Diano and in the upper Val d'Agri, we subdivided the main dataset into two sub-datasets, one to the North and the other to the south of this seismic gap area. Inversion results for the northern part, the Irpinia–Potentino area (28 fault plane solutions), show a quite similar orientation for the σ_3 principal stress axes as in the previous inversion. There is a small counter-clockwise rotation (19°) of the minimum compression stress axis, and σ_1 is more close to the vertical. The average misfit is 7.0°. In the Southern part, the Moliterno–North-western Pollino Range data (21 focal mechanisms), inversion results show a more homogeneous stress field (average misfit 6.0°) with a horizontal σ_3 NE-oriented. Both the stress inversions performed in the two adjacent areas, to the

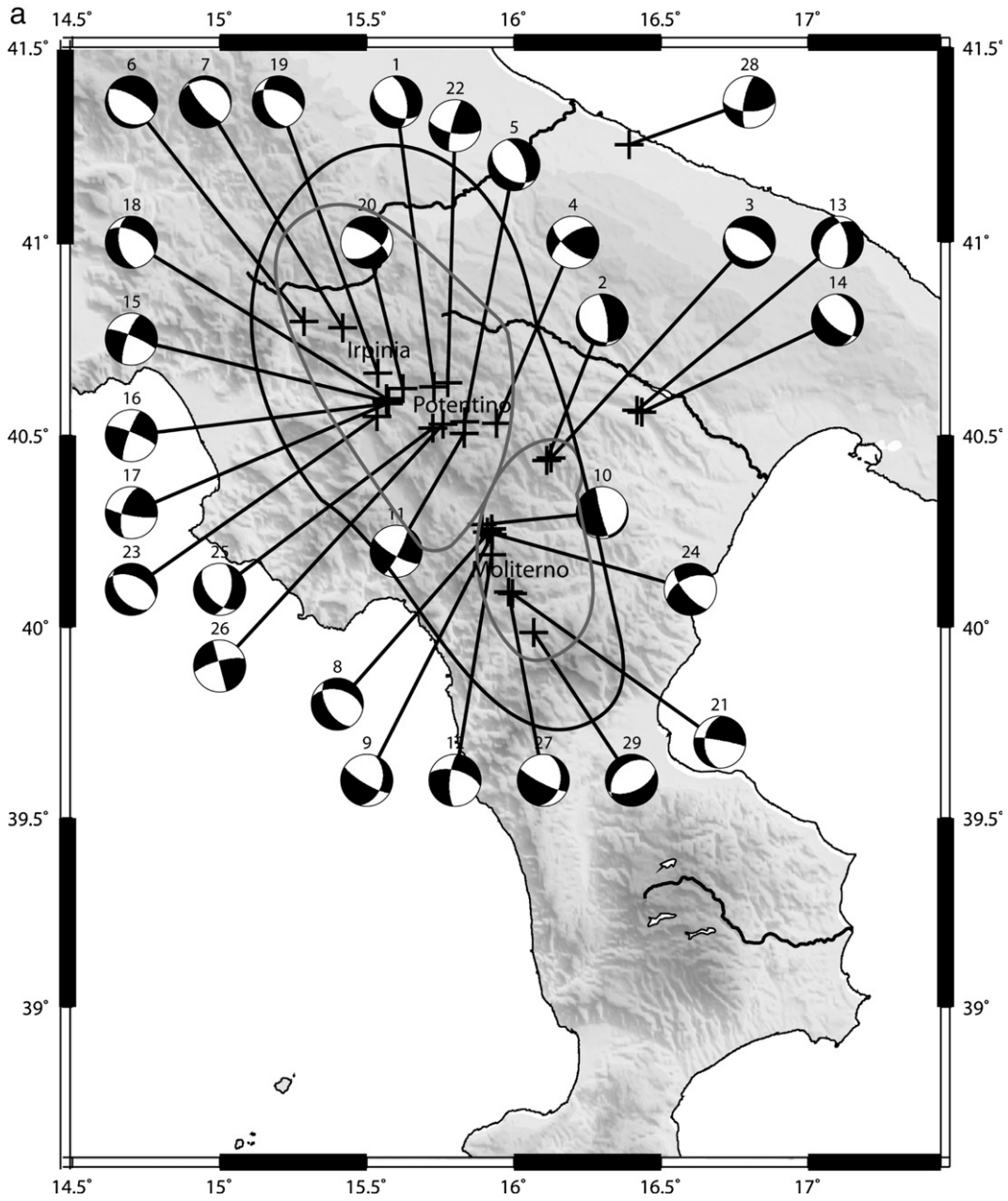

Fig. 12. a,b. Location of the 58 selected fault plane solutions. Event numbers of Table 5 are shown close to each focal mechanism. Coloured lines encircle the crustal volume considered for the stress inversion: black line for the inversion with 49 fault plane solutions; grey lines for the two inversions of the Irpinia–Potentino area to the North (28 events) and the Moliterno-North-western Pollino area to the South (21 events).

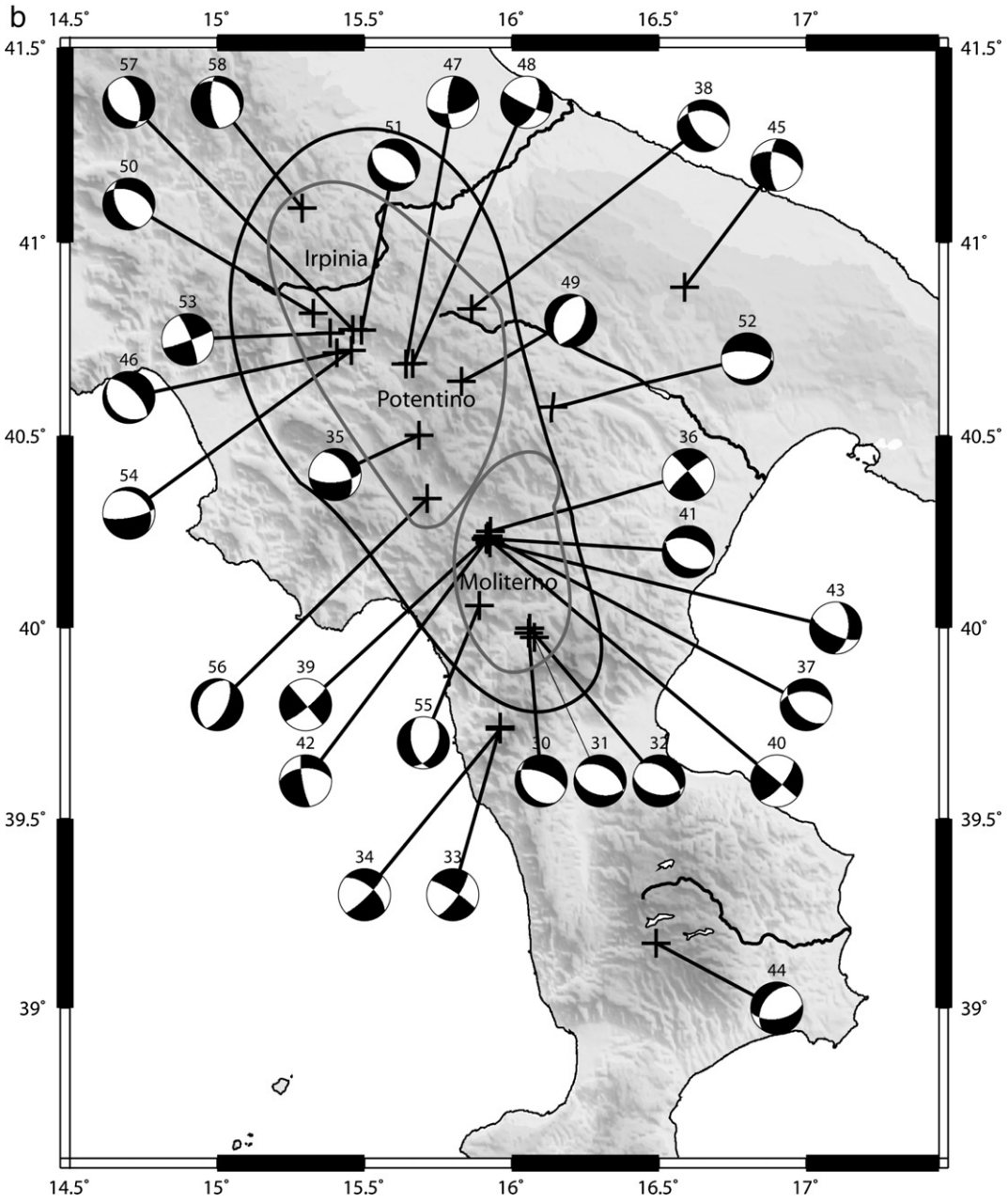

Fig. 12 (*continued*).

South and to the North, show similar results. Only the average misfit in the northern sector is quite large. This could be due to a high variability of stress in space within this area. As we know from the seismic events of 1990 and 1991, the Potentino area, which is included in the northern sector, is characterized by prevalent right-lateral strike-slip solutions (Azzara et al., 1993; Ekström, 1994) and probably suffers of the influence of the stress field change from the pure extension within the Apenninic chain to a transtension stress regime in the outer margin of the chain.

Our results are consistent with previous analysis performed in the same region (Frepoli and Amato, 2000; Frepoli et al., 2005). The SW–NE extension observed along the Southern Apennines is mainly concentrated in a relatively narrow belt (80 to 100 km wide). Within this belt the largest part of the seismic moment release is observed and most of the seismogenic faults are located. By evaluating the total seismic moment tensor of recent and historical earthquakes, we can observe an extension rate ranging from 0.3 mm/year in the Northern Apennines to 2.0 mm/year in the central and Southern Apennines (Selvaggi, 1998). Moreover, Hunstad et al. (2003) show with geodetic measurements of shear strain in a time span of 126 years that the deformation is largely confined within a region a few tens of kilometres wide. In this area is included the seismically most active part of the Apenninic chain. Regional extensional rates in the whole Apennines are in the range of 2.5 to 5 mm/year (Hunstad et al., 2003).

It is interesting to note the event located in the North-western Murge area at 23 km depth (event number 28 in Table 5) which shows a right-lateral strike-slip solution with a small thrust component. This would be a meaningful result representative of a regional field acting on the Adriatic microplate boundaries characterized by transpressive conditions (Di Luccio et al., 2005; Del Gaudio et al., 2007). The lack of pure reverse focal solutions in the Southern Foreland (Molise, Gargano and Apulia) suggests that accretion processes are not active at present.

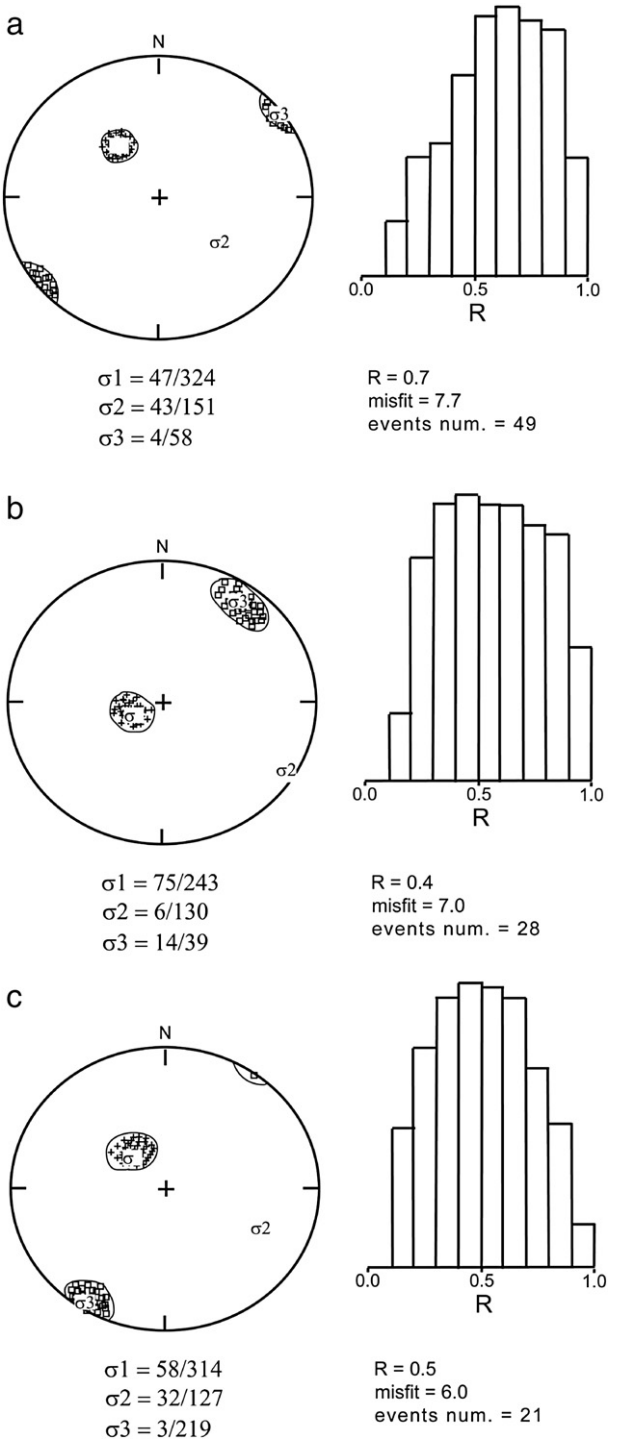

Fig. 13. Stress inversion results using: a) 49 solutions (Apenninic chain); b) 28 solutions (Irpinia–Potentino); c) 21 solutions (Moliterno–Pollino). For each inversion is shown the stereonet plot with the 95% confidence limits for σ_1 (small crosses) and σ_3 (small squares) and the histogram illustrating the uncertainty in the *R* parameter. Plunge and trend for the three principal stress axes are shown below the stereonets.

The generalized NE extension in this portion of the Southern Apennines could be explained by the buoyancy forces which are related to the westward subduction of the Adriatic continental lithosphere beneath the Apennines. Moreover, from tomographic images there is evidence of a less dense slab at depths shallower than 250 km (Amato et al., 1993; Lucente et al., 1999; Cimini and De Gori, 2001). Some studies interpret the low velocity anomalies found beneath the central-southern Apennines as a detachment in the subducting lithosphere (Spakman, 1990; Spakman et al., 1993). More recently De Gori et al. (2001), through detailed tomographic studies focused on the Southern Apennines, have pointed out the presence of an almost continuous high-velocity body extended from 65 km down to 285 km of depth. They interpreted it as Adriatic lithosphere subducted beneath the Southern Apennines. This result can be explained considering that the previous tomography images had a poor resolution at shallow depths below the studied region. Another characteristic of the Southern Apennines' subduction is the absence of a Benioff plane. Carminati et al. (2002) have suggested that the absence of seismicity at intermediate depth (60–300 km) could be related to the continental composition of the subducted Adriatic lithosphere which is expected to have ductile rather than brittle behaviour.

The results coming from present-day stress field studies, as shown in this work, give important contributions to seismotectonic zoning and seismic hazard assessment. A detailed active stress map may tell us by which mechanism faults are more likely to rupture in future events, especially in regions where active faults have no surface expression as in some parts of Southern Italy. In fact, many moderate but hazardous earthquakes occur on blind faults in the Italian region, with large repeat times of the order of thousands of years. For this reason it is important to integrate the stress field data with historical information and with seismicity patterns determined from instrumental monitoring in order to extend our possibility of assessing seismic hazard.

Acknowledgements

The present work was partially funded by Centro di Geomorfologia Integrata per l'Area del Mediterraneo (CGIAM). We thank the two anonymous reviewers for the constructive remarks that improved the work. The GMT graphics software (Wessel and Smith, 1991) has been used for some of the figures.

References

Amato, A., Alessandrini, B., Cimini, G.B., Frepoli, A., Selvaggi, G., 1993. Active and remnant subducted slabs beneath Italy: evidence from seismic tomography and seismicity. Ann. Geofis. 36 (2), 201–214.

Argus, D.F., Gordon, R.G., DeMets, C., Stein, S., 1989. Closure of the Africa–Eurasia–North America plate motion circuit and tectonics of the Gloria Fault. J. Geophys. Res. 94 (B5), 5585–5602.

Azzara, R., Basili, A., Beranzoli, L., Chiarabba, C., Di Giovambattista, R., Selvaggi, G., 1993. The seismic sequence of Potenza (May 1990). Ann. Geofis. 36 (1), 237–243.

Barberi, G., Casentino, M.T., Gervasi, A., Guerra, I., Neri, G., Orecchio, B., 2004. Crustal seismic tomography in the Calabrian Arc region, south, Italy. Phys. Earth Planet. Inter. 147, 297–314.

Bassin, C., Laske, G., Masters, G., 2000. The current limits of resolution for surface wave tomography in North America. EOS Trans AGU 81, F897.

Bigi, G., Cosentino, D., Parotto, M., Sartori, R., Scandone, P., 1990. Structural model of Italy 1:500.000. PFG-CNR, Quad. Ric. Sci., p. 114.

Boschi, E., Pantosti, D., Slejko, D., Stucchi, M., Valensise, G. (Eds.), 1990. Irpinia dieci anni dopo. Ann. Geofis., XXXVI(1), p. 363.

Carminati, E., Giardini, F., Doglioni, C., 2002. Rheological control on subcrustal seismicity in the Apennines subduction (Italy). Geophys. Res. Lett. 29 (18). doi:10.1029/2001GL014084 1882.

Cassinis, R., Scarascia, S., Lozej, A., 2003. The deep crustal structure of Italy and surrounding areas from seismic refraction data. A new synthesis. Boll. Soc. Geol. Ital. 122, 365–376.

Castello, B., Selvaggi, G., Chiarabba, C., Amato, A., 2005. CSI Catalogo della sismicità italiana 1981–2002. Versione 1.0 (INGV-CNT, Roma). on line: http://www.ingv.it/CSI/.

Chatelain, J.L., 1978. Etude fine de la sismicité en zone de collision continentale à l'aide d'un réseau de statios portables: la region Hindu-Kush-Pamir. Thèse de 3 éme cycle, Univ. Paul Sabatier, Toulouse.

Chiarabba, C., Amato, A., 1996. Crustal velocity structure of the Apennines (Italy) from P-wave travel time tomography. Ann. Geofis. XXXIX (6), 1133–1148.

Chiarabba, C., Frepoli, A., 1997. Minimum 1D velocity models in Central and Southern Italy: a contribution to better constrain hypocentral determinations. Ann. Geofis. XL (4), 937–954.

Chiarabba, C., Jovane, L., Di Stefano, R., 2005. A new view of Italian seismicity using 20 years of instrumental recordings. Tectonophysics 395, 251–268. doi:10.1016/j.tecto.2004.09.013.

Cimini, G.B., De Gori, P., 2001. Nonlinear P-wave tomography of subducted lithosphere beneath central-southern Apennines (Italy). Geophys. Res. Lett. 28 (23), 4387–4390.
Cimini, G.B., De Gori, P., Frepoli, A., 2006. Passive seismology in Southern Italy: the SAPTEX array. Ann. Geofis. 49 (2/3), 825–840.
CPTI Working Group, 1999. Catalogo Parametrico dei Forti terremoti Italiani (GNDT-ING-SGA-SSN). (Ed. Compositori, Bologna), pp.88.
Cucci, L., Pondrelli, S., Frepoli, A., Mariucci, M.T., Moro, M., 2004. Local pattern of stress field and seismogenic sources in the Pergola–Melandro Basin and the Agri Valley (Southern Italy). Geophys. J. Int. 156 (3), 575–583. doi:10.1111/j.1365-246X.2004.02161.x.
D'Agostino, N., Selvaggi, G., 2004. Crustal motion along the Eurasia–Nubia plate boundary in the Calabrian Arc and Sicily and active extension in the Messina Straits from GPS measurements. J. Geophys. Res. 109, B11402. doi:10.1029/2004JB002998.
De Gori, P., Cimini, G.B., Chiarabba, C., De Natale, G., Troie, C., Deschamps, A., 2001. Teleseismic tomography of the Campanian volcanic area and surrounding Apenninic belt. J. Volcanol. Geotherm. Res. 109, 55–75.
Del Gaudio, V., Pierri, P., Frepoli, A., Calcagnite, G., Venisti, N., Cimini, G.B., 2007. A critical revision of the seismicity of Northern Apulia (Adriatic microplate–Southern Italy) and implications for the identification of seismogenic structures. Tectonophysics 436, 9–35. doi:10.1016/j.tecto.2007.02.013.
De Mets, C., Gordon, R.G., Argus, D.F., Stein, S., 1990. Current plate motions. Geophys. J. Int. 104, 73–74.
Di Luccio, F., Fukuyama, E., Pino, N.A., 2005. The 2002 Molise earthquake sequence: what can we learn about the tectonics of Southern Italy? Tectonophysics 405, 141–154. doi:10.1016/j.tecto.2005.05.024.
Ekström, G., 1994. Teleseismic analysis of the 1990 and 1991 earthquakes near Potenza. Ann. Geofis. 37 (6), 1591–1599.
Frepoli, A., Amato, A., 2000. Fault plane solutions of crustal earthquakes in Southern Italy (1988–1995): seismotectonic implications. Ann. Geofis. 43 (3), 437–467.
Frepoli, A., Cinti, F.R., Amicucci, L., Cimini, G.B., De Gori, P., Pierdominici, S., 2005. Pattern of seismicity in the Lucanian Apennines and foredeep (Southern Italy) from recording by SAPTEX temporary array. Ann. Geofis. 48 (6), 1035–1054.
Gentile, G.F., Bressan, G., Burlini, L., De Franco, R., 2000. Three-dimensional V_P and V_P/V_S models of the upper crust in the Friuli area (northeastern Italy). Geophys. J. Int. 141, 457–478.
Gephart, J.W., 1990. FMSI: a Fortran program for inverting fault/slickenside and earthquake focal mechanism data to obtain the regional stress tensor. Comput. Geosci. 16, 953–989.
Gephart, J.W., Forsyth, D.W., 1984. An improved method for determining the regional stress tensor using earthquake focal mechanism data: application to the San Fernando earthquake sequence. J. Geophys. Res. 89 (B11), 9305–9320.
Harabaglia, P., Monelli, F., Zito, G., 1997. Geothermics of the Apennines subduction. Ann. Geofis. XL (5), 1261–1274.
Hollenstein, Ch., Kahle, H.-G, Geiger, A., Jenny, S., Goes, S., Giardini, D., 2003. New GPS constraints on the Africa–Eurasia plate boundary zone in southern Italy. Geophys. Res. Lett. 30 (18). doi:10.1029/2003GL017554 (1935).
Hunstad, I., Selvaggi, G., D, Agostino, N., England, P., Clarke, P., Pierozzi, M., 2003. Geodetic strain in peninsular Italy between 1875 and 2001. Geophys. Res. Lett. 30 (4), 1181. doi:10.1029/2002GL016447.
Hyppolite, J.C., Angelier, J., Roure, F., 1994. A major geodynamic change revealed by quaternary stress patterns in the Southern Apennines (Italy). Tectonophysics 230, 199–210.
Kissling, E., Ellsworth, W.L., Eberhart-Phillips, D., Kradolfer, U., 1995. Initial reference models in local earthquake tomography. J. Geophys. Res. 99, 19635–19646.
Lahr, J.C., 1989. HYPOELLIPSE/version 2.0: a computer program for determining local earthquake hypocentral parameters, magnitude, and first motion pattern. U. S. Geol. Surv. Open File Rep. 95, 89–116.
Locardi, E., Nicolich, R., 1988. Geodinamica del Tirreno e dell'Appennino centromeridionale, la nuova carta della Moho. Mem. Soc. Geol. Ital. 41, 121–140.
Lucente, F.P., Chiarabba, C., Cimini, G.B., Giardini, D., 1999. Tomographic constraints on the geodynamic evolution of the Italian region. J. Geophys. Res. 104 (B9), 20,307–20,328.
Malinverno, A., Ryan, W.B.F., 1986. Extension in the Tyrrhenina Sea and shortening in the Apennines as result of arc migration driven by sinking of the lithosphere. Tectonics 5, 227–245.
Maschio, L., Ferranti, L., Burrato, P., 2005. Active extension in Val d'Agri area, southern Apennines, Italy: implications for the geometry of the seismogenic belt. Geophys. J. Int. 162, 591–609.
Merlini, S., Cippitelli, G., 2001. Structural Styles Inferred by Seismic Profiles. In: Vai, G.B., Martini, I.P. (Eds.), Anatomy of an Orogen: The Apennines and Adjacent Mediterranean Basins. Kluwer Academic Publishers, pp. 441–454.
Michetti, A.M., Ferrelli, L., Esposito, E., Porfido, E., Blumetti, A.M., Vittori, E., Serva, L., Roberts, G.P., 2000. Ground effects during the 9 September 1998, Mw=5.6, Lauria earthquake and the seismic potential of the "aseismic" Pollino region in Southern Italy. Seismol. Res. Lett. 41 (1), 31–46.
Montone, P., Mariucci, M.T., Pondrelli, S., Amato, A., 2004. An improved stress map for Italy and surrounding regions (Central Mediterranean). J. Geophys. Res. 109. doi:10.1029/2003JB002703.
Morelli, C., 1997. Recent deeper geophysical results better account for the tectonics in the Italian area. Ann. Geofis. XL (5), 1345–1358.
Morelli, C., 2000. The themes of crustal research in Italy and the role of DSS-WA seismics. Boll. Soc. Geol. Ital. 119, 141–148.
Pontoise, B., Monfret, T., 2004. Shallow seismogenic zone detected from an offshore–onshore temporary seismic network in the Esmeraldas area (Northern Ecuador). Geochem. Geophys. Geosyst. 5 (2), 1–22.
Pondrelli, S., Morelli, A., Ekström, G., Mazza, S., Boschi, E., Dziewonski, A.M., 2002. European–Mediterranean regional centroid-moment tensor:1997–2000. Phys. Earth Planet. Int. 130, 71–101.
Reasenberg, P., Oppenheimer, D., 1985. FPFIT, FPPLOT and FPPAGE: FORTRAN computer programs for calculating and displaying earthquake fault-plane solutions. U.S. Geol. Surv. Open-File Rep. 85–739.
Scrocca, D., Carminati, E., Doglioni, C., 2005. Deep structure of southern Apennines, Italy: thin-skinned or thick-skinned? Tectonics 24, 1–20. doi:10.1029/2004TC001634.
Selvaggi, G., 1998. Spatial distribution of horizontal seismic strain in the Apennines from historical earthquakes. Ann. Geofis. 41, 241–251.
Spakman, W., 1990. Tomography images of the upper mantle below central Europe and the Mediterranean. Terra Nova 2, 542–553.
Spakman, W., Van der Lee, S., Van der Hilst, R., 1993. Travel-time tomography of the European–Mediterranean mantle down to 1400 km. Phys. Earth Planet. Int. 79, 3–74.
Speranza, F., Chiappini, M., 2002. Thick-skinned tectonics in the external Apennines, Italy: new evidence from magnetic anomaly analysis. J. Geophys. Res. 107 (B11), 2290. doi:10.1029/2000JB000027.
Tesauro, M., Kaban, M.K., Cloetingh, S.A.P.L., 2008. EuCRUST-07: a new reference model for the European crust. Geophys. Res. Lett. 35 (5). doi:10.1029/2007GL032244.
Tiberti, M.M., Orlando, L., Bucci, D., Bernarbini, M., Parotto, M., 2005. Regional gravity anomaly map and crustal model of the Central–Southern Apennines (Italy). Journal of Geodynamics 40, 73–91. doi:10.1016/j.jog.2005.07.014.
Ventura, G., Cinti, F.R., Di Luccio, F., Pino, N.A., 2007. Mantle wedge dynamics versus crustal seismicity in the Apennines (Italy). Geochem. Geophys. Geosyst. 8 (2), 1525–2027. doi:10.1029/2006GC001421.
Wessel, P., Smith, W.H.F., 1991. Free software helps map and display data, EOS Trans. AGU 72, 445–446.
Wyss, M., Liang, B., Tanigawa, W.R., Wu, X., 1992. Comparison of orientations of stress and strain tensors based on fault-plane solutions in Kaoiki, Hawaii. J. Geophys. Res. 97, 4769–4790.